Charge-Dependent Directed Flow in Cu + Au Collisions at $\sqrt{s_{NN}} = 200$ GeV

L. Adamczyk,[1] J. K. Adkins,[20] G. Agakishiev,[18] M. M. Aggarwal,[32] Z. Ahammed,[50] I. Alekseev,[16,27] D. M. Anderson,[43] R. Aoyama,[3] A. Aparin,[18] D. Arkhipkin,[3] E. C. Aschenauer,[3] M. U. Ashraf,[46] A. Attri,[32] G. S. Averichev,[18] X. Bai,[7] V. Bairathi,[28] R. Bellwied,[45] A. Bhasin,[17] A. K. Bhati,[32] P. Bhattarai,[44] J. Bielcik,[10] J. Bielcikova,[11] L. C. Bland,[3] I. G. Bordyuzhin,[16] J. Bouchet,[19] J. D. Brandenburg,[37] A. V. Brandin,[27] I. Bunzarov,[18] J. Butterworth,[37] H. Caines,[54] M. Calderón de la Barca Sánchez,[5] J. M. Campbell,[30] D. Cebra,[5] I. Chakaberia,[3] P. Chaloupka,[10] Z. Chang,[43] A. Chatterjee,[50] S. Chattopadhyay,[50] X. Chen,[22] J. H. Chen,[40] J. Cheng,[46] M. Cherney,[9] W. Christie,[3] G. Contin,[23] H. J. Crawford,[4] S. Das,[13] L. C. De Silva,[9] R. R. Debbe,[3] T. G. Dedovich,[18] J. Deng,[39] A. A. Derevschikov,[34] B. di Ruzza,[3] L. Didenko,[3] C. Dilks,[33] X. Dong,[23] J. L. Drachenberg,[21] J. E. Draper,[5] C. M. Du,[22] L. E. Dunkelberger,[6] J. C. Dunlop,[3] L. G. Efimov,[18] J. Engelage,[4] G. Eppley,[37] R. Esha,[6] S. Esumi,[3] O. Evdokimov,[8] O. Eyser,[3] R. Fatemi,[20] S. Fazio,[3] P. Federic,[11] J. Fedorisin,[18] Z. Feng,[7] P. Filip,[18] E. Finch,[47] Y. Fisyak,[3] C. E. Flores,[5] L. Fulek,[1] C. A. Gagliardi,[43] D. Garand,[35] F. Geurts,[37] A. Gibson,[49] M. Girard,[51] L. Greiner,[23] D. Grosnick,[49] D. S. Gunarathne,[42] Y. Guo,[38] S. Gupta,[17] A. Gupta,[17] W. Guryn,[3] A. I. Hamad,[19] A. Hamed,[43] R. Haque,[28] J. W. Harris,[54] L. He,[35] S. Heppelmann,[33] S. Heppelmann,[5] A. Hirsch,[35] G. W. Hoffmann,[44] S. Horvat,[54] B. Huang,[8] X. Huang,[46] H. Z. Huang,[6] T. Huang,[29] P. Huck,[7] T. J. Humanic,[30] G. Igo,[6] W. W. Jacobs,[15] A. Jentsch,[44] J. Jia,[3,41] K. Jiang,[38] S. Jowzaee,[52] E. G. Judd,[4] S. Kabana,[19] D. Kalinkin,[15] K. Kang,[46] K. Kauder,[52] H. W. Ke,[3] D. Keane,[19] A. Kechechyan,[18] Z. H. Khan,[8] D. P. Kikoła,[51] I. Kisel,[12] A. Kisiel,[51] L. Kochenda,[27] D. D. Koetke,[49] L. K. Kosarzewski,[51] A. F. Kraishan,[42] P. Kravtsov,[27] K. Krueger,[2] L. Kumar,[32] M. A. C. Lamont,[3] J. M. Landgraf,[3] K. D. Landry,[6] J. Lauret,[3] A. Lebedev,[3] R. Lednicky,[18] J. H. Lee,[3] Y. Li,[46] C. Li,[38] W. Li,[40] X. Li,[42] X. Li,[38] T. Lin,[15] M. A. Lisa,[30] Y. Liu,[43] F. Liu,[7] T. Ljubicic,[3] W. J. Llope,[52] M. Lomnitz,[19] R. S. Longacre,[3] X. Luo,[7] S. Luo,[8] G. L. Ma,[40] R. Ma,[3] Y. G. Ma,[40] L. Ma,[40] N. Magdy,[41] R. Majka,[54] A. Manion,[23] S. Margetis,[19] C. Markert,[44] H. S. Matis,[23] D. McDonald,[45] S. McKinzie,[23] K. Meehan,[5] J. C. Mei,[39] Z. W. Miller,[8] N. G. Minaev,[34] S. Mioduszewski,[43] D. Mishra,[28] B. Mohanty,[28] M. M. Mondal,[43] D. A. Morozov,[34] M. K. Mustafa,[23] B. K. Nandi,[14] Md. Nasim,[6] T. K. Nayak,[50] G. Nigmatkulov,[27] T. Niida,[52] L. V. Nogach,[34] T. Nonaka,[3] J. Novak,[26] S. B. Nurushev,[34] G. Odyniec,[23] A. Ogawa,[3] K. Oh,[36] V. A. Okorokov,[27] D. Olvitt Jr,[42] B. S. Page,[3] R. Pak,[3] Y. X. Pan,[6] Y. Pandit,[8] Y. Panebratsev,[18] B. Pawlik,[31] H. Pei,[7] C. Perkins,[4] P. Pile,[3] J. Pluta,[51] K. Poniatowska,[51] J. Porter,[23] M. Posik,[42] A. M. Poskanzer,[23] N. K. Pruthi,[32] M. Przybycien,[1] J. Putschke,[52] H. Qiu,[35] A. Quintero,[42] S. Ramachandran,[20] R. L. Ray,[44] R. Reed,[24,24] M. J. Rehbein,[9] H. G. Ritter,[23] J. B. Roberts,[37] O. V. Rogachevskiy,[18] J. L. Romero,[5] J. D. Roth,[9] L. Ruan,[3] J. Rusnak,[11] O. Rusnakova,[10] N. R. Sahoo,[43] P. K. Sahu,[13] I. Sakrejda,[23] S. Salur,[23] J. Sandweiss,[54] A. Sarkar,[14] J. Schambach,[44] R. P. Scharenberg,[35] A. M. Schmah,[23] W. B. Schmidke,[3] N. Schmitz,[25] J. Seger,[9] P. Seyboth,[25] N. Shah,[40] E. Shahaliev,[18] P. V. Shanmuganathan,[19] M. Shao,[38] A. Sharma,[17] M. K. Sharma,[17] B. Sharma,[32] W. Q. Shen,[40] S. S. Shi,[7] Z. Shi,[23] Q. Y. Shou,[40] E. P. Sichtermann,[23] R. Sikora,[1] M. Simko,[11] S. Singha,[19] M. J. Skoby,[15] D. Smirnov,[3] N. Smirnov,[54] W. Solyst,[15] L. Song,[45] P. Sorensen,[3] H. M. Spinka,[2] B. Srivastava,[35] T. D. S. Stanislaus,[49] M. Stepanov,[35] R. Stock,[12] M. Strikhanov,[27] B. Stringfellow,[35] T. Sugiura,[3] M. Sumbera,[11] B. Summa,[33] Z. Sun,[22] Y. Sun,[38] X. M. Sun,[7] B. Surrow,[42] D. N. Svirida,[16] A. H. Tang,[3] Z. Tang,[38] T. Tarnowsky,[26] A. Tawfik,[53] J. Thäder,[23] J. H. Thomas,[23] A. R. Timmins,[45] D. Tlusty,[37] T. Todoroki,[3] M. Tokarev,[18] S. Trentalange,[6] R. E. Tribble,[43] P. Tribedy,[3] S. K. Tripathy,[13] O. D. Tsai,[6] T. Ullrich,[3] D. G. Underwood,[2] I. Upsal,[30] G. Van Buren,[3] G. van Nieuwenhuizen,[3] R. Varma,[14] A. N. Vasiliev,[34] R. Vertesi,[11] F. Videbæk,[3] S. Vokal,[18] S. A. Voloshin,[52] A. Vossen,[15] G. Wang,[6] F. Wang,[35] J. S. Wang,[22] Y. Wang,[7] H. Wang,[3] Y. Wang,[46] J. C. Webb,[3] G. Webb,[3] L. Wen,[6] G. D. Westfall,[26] H. Wieman,[23] S. W. Wissink,[15] R. Witt,[48] Y. Wu,[19] Z. G. Xiao,[46] W. Xie,[35] G. Xie,[38] K. Xin,[37] Q. H. Xu,[39] Y. F. Xu,[40] H. Xu,[22] Z. Xu,[3] N. Xu,[23] J. Xu,[7] C. Yang,[38] Y. Yang,[7] S. Yang,[38] Y. Yang,[29] Q. Yang,[38] Y. Yang,[22] Z. Ye,[8] Z. Ye,[8] L. Yi,[54] K. Yip,[3] I. -K. Yoo,[36] N. Yu,[7] H. Zbroszczyk,[51] W. Zha,[38] J. Zhang,[22] X. P. Zhang,[46] S. Zhang,[38] Y. Zhang,[38] J. B. Zhang,[7] Z. Zhang,[40] S. Zhang,[40] J. Zhang,[39] J. Zhao,[35] C. Zhong,[40] L. Zhou,[38] X. Zhu,[46] Y. Zoulkarneeva,[18] and M. Zyzak[12]

(STAR Collaboration)

[1]*AGH University of Science and Technology, FPACS, Cracow 30-059, Poland*
[2]*Argonne National Laboratory, Argonne, Illinois 60439, USA*
[3]*Brookhaven National Laboratory, Upton, New York 11973, USA*
[4]*University of California, Berkeley, California 94720, USA*
[5]*University of California, Davis, California 95616, USA*

[6]University of California, Los Angeles, California 90095, USA
[7]Central China Normal University, Wuhan, Hubei 430079, China
[8]University of Illinois at Chicago, Chicago, Illinois 60607, USA
[9]Creighton University, Omaha, Nebraska 68178, USA
[10]Czech Technical University in Prague, FNSPE, Prague, 115 19, Czech Republic
[11]Nuclear Physics Institute AS CR, 250 68 Prague, Czech Republic
[12]Frankfurt Institute for Advanced Studies FIAS, Frankfurt 60438, Germany
[13]Institute of Physics, Bhubaneswar 751005, India
[14]Indian Institute of Technology, Mumbai 400076, India
[15]Indiana University, Bloomington, Indiana 47408, USA
[16]Alikhanov Institute for Theoretical and Experimental Physics, Moscow 117218, Russia
[17]University of Jammu, Jammu 180001, India
[18]Joint Institute for Nuclear Research, Dubna, 141 980, Russia
[19]Kent State University, Kent, Ohio 44242, USA
[20]University of Kentucky, Lexington, Kentucky 40506-0055, USA
[21]Lamar University, Physics Department, Beaumont, Texas 77710, USA
[22]Institute of Modern Physics, Chinese Academy of Sciences, Lanzhou, Gansu 730000, China
[23]Lawrence Berkeley National Laboratory, Berkeley, California 94720, USA
[24]Lehigh University, Bethlehem, Pennsylvania 18015, USA
[25]Max-Planck-Institut fur Physik, Munich 80805, Germany
[26]Michigan State University, East Lansing, Michigan 48824, USA
[27]National Research Nuclear University MEPhI, Moscow 115409, Russia
[28]National Institute of Science Education and Research, Bhubaneswar 751005, India
[29]National Cheng Kung University, Tainan 70101, Taiwan
[30]Ohio State University, Columbus, Ohio 43210, USA
[31]Institute of Nuclear Physics PAN, Cracow 31-342, Poland
[32]Panjab University, Chandigarh 160014, India
[33]Pennsylvania State University, University Park, Pennsylvania 16802, USA
[34]Institute of High Energy Physics, Protvino 142281, Russia
[35]Purdue University, West Lafayette, Indiana 47907, USA
[36]Pusan National University, Pusan 46241, Korea
[37]Rice University, Houston, Texas 77251, USA
[38]University of Science and Technology of China, Hefei, Anhui 230026, China
[39]Shandong University, Jinan, Shandong 250100, China
[40]Shanghai Institute of Applied Physics, Chinese Academy of Sciences, Shanghai 201800, China
[41]State University Of New York, Stony Brook, New York 11794, USA
[42]Temple University, Philadelphia, Pennsylvania 19122, USA
[43]Texas A&M University, College Station, Texas 77843, USA
[44]University of Texas, Austin, Texas 78712, USA
[45]University of Houston, Houston, Texas 77204, USA
[46]Tsinghua University, Beijing 100084, China
[47]Southern Connecticut State University, New Haven, Connecticut 06515, USA
[48]United States Naval Academy, Annapolis, Maryland 21402, USA
[49]Valparaiso University, Valparaiso, Indiana 46383, USA
[50]Variable Energy Cyclotron Centre, Kolkata 700064, India
[51]Warsaw University of Technology, Warsaw 00-661, Poland
[52]Wayne State University, Detroit, Michigan 48201, USA
[53]World Laboratory for Cosmology and Particle Physics (WLCAPP), Cairo 11571, Egypt
[54]Yale University, New Haven, Connecticut 06520, USA

(Received 13 August 2016; revised manuscript received 20 October 2016; published 5 January 2017)

We present the first measurement of charge-dependent directed flow in Cu + Au collisions at $\sqrt{s_{NN}} = 200$ GeV. The results are presented as a function of the particle transverse momentum and pseudorapidity for different centralities. A finite difference between the directed flow of positive and negative charged particles is observed that qualitatively agrees with the expectations from the effects of the initial strong electric field between two colliding ions with different nuclear charges. The measured difference in directed flow is much smaller than that obtained from the parton-hadron-string-dynamics model, which suggests that most of the electric charges, i.e., quarks and antiquarks,

have not yet been created during the lifetime of the strong electric field, which is of the order of, or less than, 1 fm/c.

DOI: 10.1103/PhysRevLett.118.012301

Hot and dense nuclear matter has been extensively studied in nucleus-nucleus collisions at the Relativistic Heavy Ion Collider (RHIC) [1–4] and the Large Hadron Collider (LHC) [5–7]. Numerous experimental results have suggested that a quark-gluon plasma (QGP) consisting of deconfined quarks and gluons is created in these collisions. At present, the emphasis is on characterizing the detailed properties of the QGP.

One of the most important and informative experimental observables used to study the properties of the QGP is the azimuthal anisotropic flow, which can be characterized by the Fourier coefficients extracted from the azimuthal distribution of the final state particles [8]. The second-order Fourier coefficient (so called elliptic flow) and higher-order Fourier coefficients v_n $(n > 2)$ are found to be very sensitive to the shear viscosity over entropy density ratio η/s [9,10]. The first-order Fourier coefficient v_1, also known as directed flow, is sensitive to the equation of state of the medium and therefore could be a possible probe of a QGP phase transition [11–13].

Recent theoretical studies suggest that an asymmetric colliding system can provide new insights regarding the properties of a QGP, such as the electric conductivity [14] and the time evolution of the quark densities [15]. Figure 1 shows an example of the distribution of spectators and participants (protons and neutrons) in the transverse plane for a Cu + Au collision assuming an impact parameter of 6 fm. Because of the difference in the number of protons in the two nuclei, a strong electric field is created at the initial stage of the collision and the direction of the field is indicated by the arrow in Fig. 1. The lifetime of the field might be very short, of the order of a fraction of 1 fm/c (e.g., $t \sim 0.25$ fm/c from Ref. [14,15]), but the electric charges from quarks and antiquarks that are present in the early stage of the collision would experience the Coulomb force and so would be pushed along or opposite to the field direction depending on the particle charge. The azimuthal distribution of produced particles (including the effect of the electric field) can be written as [14,16]

$$\frac{dN^{\pm}}{d\phi} \propto 1 + 2v_1 \cos(\phi - \Psi_1) \pm 2d_E \cos(\phi - \psi_E) \cdots, \quad (1)$$

where ϕ is the azimuthal angle for a particle, Ψ_1 is the angle of orientation for the first-order event plane, and the upper (lower) sign of $\pm$ is for the positively (negatively) charged particles. ψ_E denotes the azimuthal angle of the electric field; it is strongly correlated with Ψ_1 (see Fig. 1) but can differ from Ψ_1 event by event due to the fluctuation of the initial nucleon distribution. The coefficient d_E characterizes the strength of dipole deformation induced by the electric field and is proportional to the electric conductivity of the plasma. Then the directed flow v_1 of positively and negatively charged particles can be expressed as

$$v_1^{\pm} = v_1 \pm d_E \langle \cos(\Psi_1 - \psi_E) \rangle, \quad (2)$$

where $\langle\rangle$ means an average over all particles in all events. Equation (2) illustrates how the presence of an electric field results in charge separation for directed flow. The strength of the charge separation depends on the number of (anti) quarks existing at the earliest stages of the collision when the electric field is strong. Therefore, the measurement of charge-dependent directed flow can be used to test the quark production mechanism, such as the two-wave scenario of quark production [17,18]. Also, understanding the time evolution of the quark density in heavy-ion collisions is very important for a detailed theoretical prediction of the chiral magnetic effect [19,20] and the chiral magnetic wave [21,22]. These effects are supposed to emerge under an initial strong magnetic field and are actively searched for by various experiments [23–27].

In this Letter, we present the first measurement of the charge-dependent directed flow in Cu + Au collisions at $\sqrt{s_{NN}} = 200$ GeV. The results are presented for different collision centralities as a function of the particle transverse momentum p_T and pseudorapidity η. For comparison we also show results for Au + Au collisions where the effect is

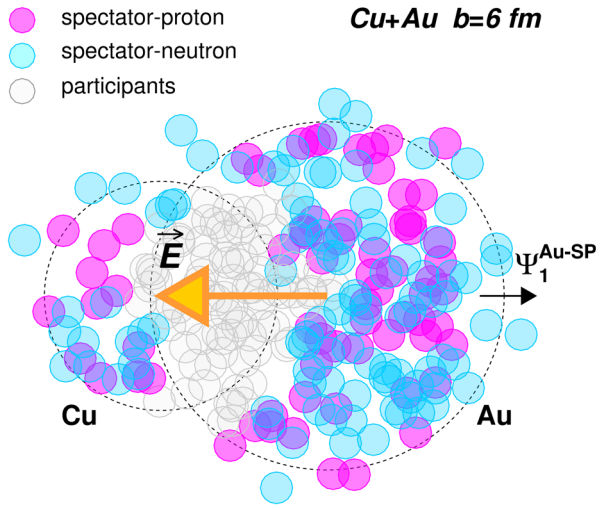

FIG. 1. Example of a noncentral Cu + Au collision viewed in the transverse plane showing an initial electric field $\vec{E}$ caused by the charge difference between two nuclei. $\Psi_1^{\text{Au-SP}}$ denotes the direction of Au spectators.

expected to be significantly smaller, because the average electric field in these collisions is expected to be zero.

The data reported in this analysis are from Cu + Au collisions at $\sqrt{s_{NN}} = 200$ GeV collected in 2012 with the STAR detector. The collision vertices were reconstructed using charged-particle tracks measured in the time projection chamber (TPC) [28]. The TPC covers the full azimuth and has a pseudorapidity range of $|\eta| < 1.0$. Events were selected to have the collision vertex position within ± 30 cm from the center of the TPC in the beam direction and within ± 2 cm in the radial direction with respect to the center of the beam. An additional constraint on the vertex position along the beam direction was imposed using the vertex position detector [29] to reduce the beam-induced background. Forty-four $\times 10^6$ minimum bias Cu + Au events were used in the analysis, where the minimum bias trigger required hits of vertex position detectors and zero degree calorimeters (ZDCs, described below) in Cu and Au going directions. In addition, 95×10^6 minimum bias Au + Au events, collected in 2010, were analyzed in the same way for comparison.

The centrality of each collision was determined by measuring event-by-event multiplicity and interpreting the measurement with a tuned Monte Carlo Glauber calculation [30,31]. The first-order event plane was determined by ZDCs that are equipped with shower maximum detectors (SMDs) [32–34]. The ZDC SMDs are located at forward and backward angles ($|\eta| > 6.3$) and they measure the energy deposited by spectator neutrons as well as the transverse distribution of the neutrons. It is worth noting that spectator neutrons, on average, deflect outward from the center line of the collisions [35] and thus provide information on the direction of the electric field. The event plane resolution was estimated by the three-subevent method [36]. It reaches a maximum of 0.26 for midcentral events when using the ZDC SMD in the Au-going direction. Analyzed tracks were required to have the distance of closest approach to the primary vertex to be less than 3 cm, and to have at least 15 TPC space points used in their reconstruction. Furthermore, the ratio of the number of fit points to maximum possible number of TPC space points (45) was required to be larger than 0.52 to remove split tracks. The p_T of tracks was limited to the range $0.15 < p_T < 5$ GeV/c.

Directed flow v_1 was measured using the "event plane method":

$$v_1 = \langle \cos(\phi - \Psi_1) \rangle / \mathrm{Res}\{\Psi_1\}, \quad (3)$$

where ϕ is the azimuthal angle of a track and $\mathrm{Res}\{\Psi_1\}$ denotes the event plane resolution. Directed flow is measured with respect to the spectator plane determined by the ZDC SMD in the Au-going direction, but the sign of Ψ_1 is defined to be positive at forward rapidities (Cu-going direction) to keep the convention of past v_1 measurements. Note that $v_1(\eta)$, measured with respect to the spectator plane of one of the nuclei, includes the component due to density fluctuations [37–39] and does not necessarily cross zero at $\eta = 0$ even for symmetric collisions. Also, note that η is measured in the nucleon-nucleon center-of-mass frame.

Systematic uncertainties in the results have been estimated by variation of the size of the collision z-vertex window, by variation of the track quality cuts, and by using different combinations of the three subevents in the estimation of the event plane resolution. The relative systematic uncertainties associated with the z vertex and track quality cuts are below 6% for midcentral events and were found to be uncorrelated in p_T. The uncertainty of the event plane resolution was studied by varying the detector combinations used in the three-subevent method. The detector choices were two ZDC SMD detectors, and one of the two beam beam counters [40] located at forward and backward angles ($3.3 < |\eta| < 5$), or the end cap electromagnetic calorimeter ($1.086 < \eta < 2$) [41]. The associated systematic uncertainty is p_T correlated; namely, all data points move in the same direction as the sign of v_1 with the same fraction. The change in v_1 due to the use of different subevents is ~7% for midcentral events and increases up to 22% for more central and peripheral events. This is the largest systematic uncertainty in these measurements. The Cu + Au data were taken only with one polarity of the magnetic field. In order to check the effect of the magnetic field, the Au + Au data were also analyzed with the same polarity, where no effect has been observed.

Figures 2(a)–2(e) show the directed flow of positive (h^+) and negative (h^-) charged particles as a function of p_T for five different centrality bins. The solid (dashed) lines around $v_1 = 0$ show the p_T-uncorrelated systematic uncertainties and the shaded bands, indicated with "EP," show the p_T-correlated systematic uncertainties associated with the event plane resolution. The observed v_1 has a positive value at low p_T ($p_T < 1$ GeV/c) and goes negative at high p_T.

The trend of the p_T dependence is similar to that of v_1 measured in symmetric collisions [34,39]. The magnitude of our v_1 is about 10 times larger than v_1^{even} (as shown in Fig. 3) and twice (10 times) larger than v_1^{odd} at $p_T = 1(3)$ GeV/c in Au + Au collisions [34]. This is likely because the v_1 in symmetric collisions originates only from the density fluctuations, while the v_1 in asymmetric collisions is dominated by the initial density asymmetry [42,43]. The average of v_1 for positive and negative particles is consistent, within errors, with the results of charge-combined directed flow measurements recently published by the PHENIX Collaboration [44].

Figures 2(f)–2(j) show Δv_1 defined as the difference in v_1 between positive and negative charged particles. Note that the large uncertainties on the event plane resolution largely cancel out in Δv_1. The difference Δv_1 is about 10% of v_1 in magnitude. It tends to be positive for

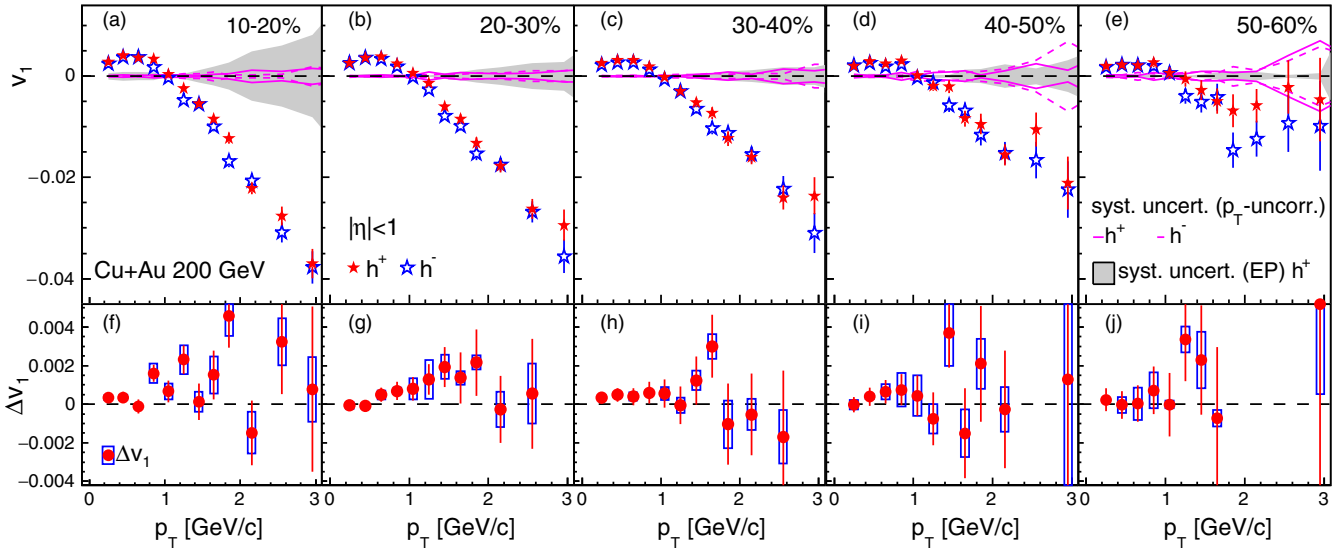

FIG. 2. Directed flow of positive and negative particles from minimum bias Cu + Au collisions at $\sqrt{s_{NN}} = 200$ GeV, as a function of p_T, in five centrality bins. The difference between the positive and negative spectra is shown in the lower panels, where the open boxes show the systematic uncertainties. See the text for the definition of the positive direction for v_1.

$p_T < 2$ GeV/c in 10%–30% centrality and becomes consistent with zero by 50%–60% centrality within large systematic uncertainties. The small but finite Δv_1 agrees with the expectation for the effects of the initial electric field. The sign flipping of the electric field discussed in Ref. [14] seems not to be observed within the current uncertainty, which is close to the expectation discussed in Ref. [16].

Figure 3 shows v_1 and Δv_1 in the 10%–40% centrality bin. For $p_T < 2$ GeV/c, the Δv_1 seems to increase with p_T. The v_1 results from Au + Au collisions (the so-called even component of v_1) show much smaller values (~by a factor of 10) compared to those in Cu + Au. Note that the odd component of v_1 in Au + Au collisions is similarly small [34]. The Δv_1 in Au + Au is consistent with zero. Calculations for charged pions from the parton-hadron-string-dynamics (PHSD) model [15], which is a dynamical transport approach in the partonic and hadronic phases, are compared to the data. As indicated in Eq. (2), the measured Δv_1 could be smeared by the fluctuations in ψ_E and Ψ_1 orientations, but note that the PHSD model takes such event-by-event fluctuations into account. The PHSD model calculates two cases: charge-dependent v_1 with and without the initial electric field (EF). For the case with the EF switched on, the model assumes that all electric charges are affected by the EF and this results in a large separation of v_1 between positive and negative particles as shown in Fig. 3(a). In Fig. 3(b), the calculations of the Δv_1 with and without the EF are shown together, but note that the EF-on data points are scaled by 0.1 relative to the PHSD results. After scaling by 0.1, the model describes rather well the p_T dependence of the measured data for $p_T < 2$ GeV/c.

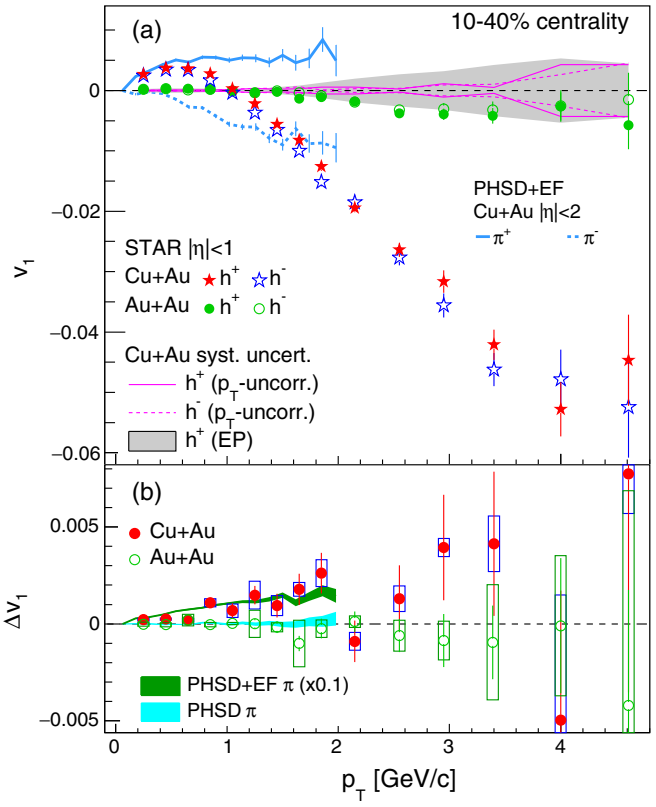

FIG. 3. Directed flow of positive and negative particles and the difference between the two spectra as a function of p_T in 10%–40% centrality in Cu + Au and Au + Au collisions. The PHSD model calculations [15] for charged pions with and without the initial electric field (EF) in the same centrality region are presented for comparison. Note that the charge difference of v_1 with the EF on is scaled by 0.1.

The magnitude of Δv_1 should depend on the number of quarks and antiquarks and the electric conductivity at the time when the EF is strong. We note, however, that the electric conductivity calculations in lattice QCD differ by an order of magnitude between different groups [45,46], and the perturbative QCD calculations [47,48] predict larger values than lattice QCD. In comparison, the electric conductivity evaluated in the PHSD model is close to the lower value of the lattice QCD calculations [49]. Therefore, the fact that the observed Δv_1 is 10 times smaller compared to the PHSD model calculation with the EF on likely indicates a small number of quarks and antiquarks at $t \leq 0.25$ fm/c. The lifetime of the electric field could be longer if the created medium is a good conductor [50–52]. Therefore, the fraction of quarks present at the early times could be even lower.

We can roughly estimate the ratio of the number of (anti)quarks that existed at very early times to the total number of (anti)quarks created in the collision (final state number) using the parton distribution functions (PDFs). We have used the HERAPDF1.5 (next-to-leading order, $Q^2 = 4$ GeV^2) parton distribution functions [53], and we assumed that the number of quarks in the initial state corresponds to the number of quarks given by the PDFs in the corresponding momentum region. We assume that the total number of hadrons in the final state is approximately equal to the number of partons in the initial state, meaning that one gluon in the initial state corresponds approximately to two quarks in the final state. Then, the ratio of the initial quarks to the total number of quarks created in the collision can be calculated by comparing the PDFs at $x \sim m_T e^{\eta}/\sqrt{s} \approx 0.01$ corresponding to the kinematics of the current measurement. Note that such an estimate depends very weakly on the exact momentum fraction range x and Q^2. Using this approach we find that the ratio is about 0.15, close to the scale factor applied to the PHSD model calculations shown in Fig. 3.

The pseudorapidity dependence of v_1 and Δv_1 was measured in the 10%–40% centrality bin as shown in Fig. 4. As seen in Figs. 2 and 3, the Δv_1 exhibits a stronger signal in the $1 < p_T < 2$ GeV/c range. Therefore, in Fig. 4 the signal is integrated over that range. The magnitude of v_1 becomes larger at forward rapidities and Δv_1 has a finite value within $|\eta| < 1$. The difference Δv_1 seems to be larger at forward rapidities (Cu-going direction). This might be related to the $v_1(y)$ (where y denotes rapidity) slope difference between particles and antiparticles [13] and the shift of the center-of-mass in asymmetric collisions, although the uncertainty of the data is still too large to discuss this in detail.

In conclusion, we have presented results for the first measurements of charge-dependent directed flow in Cu + Au collisions at $\sqrt{s_{NN}} = 200$ GeV. A finite difference in v_1 between positive and negative charged particles was observed in the transverse momentum range of

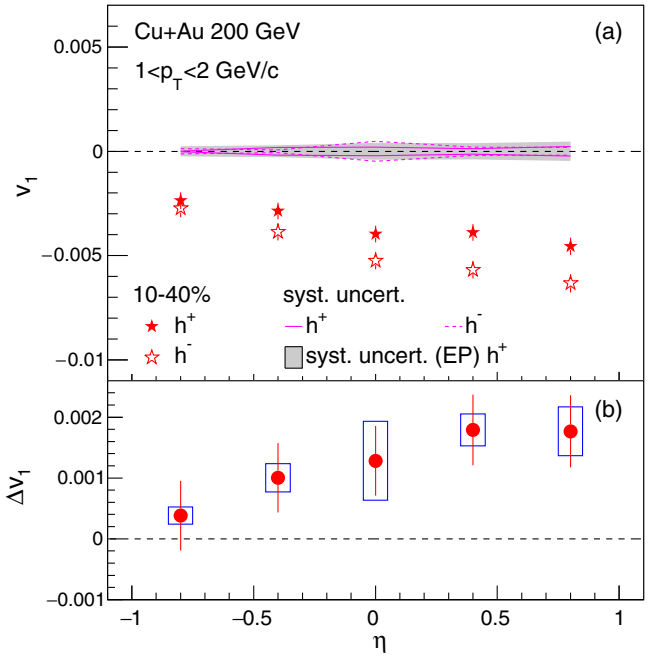

FIG. 4. Directed flow of positive and negative particles and the difference between the two spectra as a function of η in the 10%–40% centrality bin, where a positive η denotes the Cu-going direction.

$0.15 < p_T < 2$ GeV/c and the pseudorapidity range of $|\eta| < 1$. These results are consistent with the presumption of a strong, initial, electric field in asymmetric collisions. The observed Δv_1 was compared to the PHSD model calculations that include the effect of an electric field. The p_T dependence of Δv_1 is qualitatively described by the model in the region less than 2 GeV/c. However, the magnitude of Δv_1 is smaller by a factor of 10 than the model predictions, assuming that all quarks are created at the initial time. This may indicate that most of the quarks and antiquarks have not yet been created within the lifetime of the electric field ($t \leq 0.25$ fm/c). A simple estimate of the fraction of the initial quarks present in the participant nucleons, relative to all quarks created during the collision (assuming each gluon to be converted to a $q\bar{q}$ pair), is consistent with this interpretation. These results provide important information for understanding the time evolution of particle production, and will constrain estimates of the magnitude of the chiral magnetic effect and chiral magnetic wave induced by the initial strong magnetic field.

We thank the RHIC Operations Group and RCF at BNL, the NERSC Center at LBNL, and the Open Science Grid consortium for providing resources and support. This work was supported in part by the Office of Nuclear Physics within the U.S. DOE Office of Science, the U.S. National Science Foundation, the Ministry of Education and Science of the Russian Federation, National Natural Science Foundation of China, Chinese Academy of Science, the Ministry of Science and Technology of China and the

Chinese Ministry of Education, the National Research Foundation of Korea, Czech Science Foundation and Ministry of Education, Youth and Sports of the Czech Republic, Department of Atomic Energy and Department of Science and Technology of the Government of India, the National Science Centre of Poland, the Ministry of Science, Education and Sports of the Republic of Croatia, RosAtom of Russia and German Bundesministerium fur Bildung, Wissenschaft, Forschung and Technologie (BMBF) and the Helmholtz Association.

[1] K. Adcox *et al.* (PHENIX Collaboration), Formation of dense partonic matter in relativistic nucleus-nucleus collisions at RHIC: Experimental evaluation by the PHENIX collaboration, Nucl. Phys. **A757**, 184 (2005).

[2] J. Adams *et al.* (STAR Collaboration), Experimental and theoretical challenges in the search for the quark gluon plasma: The STAR Collaboration's critical assessment of the evidence from RHIC collisions, Nucl. Phys. **A757**, 102 (2005).

[3] B. B. Back *et al.* (PHOBOS Collaboration), The PHOBOS perspective on discoveries at RHIC, Nucl. Phys. **A757**, 28 (2005).

[4] l. Arsene *et al.* (BRAHMS Collaboration), Quark gluon plasma an color glass condensate at RHIC? The perspective from the BRAHMS experiment, Nucl. Phys. **A757**, 1 (2005).

[5] K. Aamodt *et al.* (ALICE Collaboration), Suppression of charged particle production at large transverse momentum in central Pb + Pb collisions at $\sqrt{s_{NN}} = 2.76$ TeV, Phys. Lett. B **696**, 30 (2011).

[6] S. Chatrchyan *et al.* (CMS Collaboration), Observation and studies of jet quenching in PbPb collisions at $\sqrt{s_{NN}} = 2.76$ TeV, Phys. Rev. C **84**, 024906 (2011).

[7] G. Aad *et al.* (ATLAS Collaboration), Observation of a Centrality-Dependent Dijet Asymmetry in Lead-Lead Collisions at $\sqrt{s_{NN}} = 2.76$ TeV with the ATLAS Detector, Phys. Rev. Lett. **105**, 252303 (2010).

[8] S. A. Voloshin, A. M Poskanzer, and R. Snellings, Collective phenomena in non-central nuclear collisions, arXiv: 0809.2949.

[9] A. Adare *et al.* (PHENIX Collaboration), Measurements of Higher Order Flow Harmonics in Au + Au Collisions at $\sqrt{s_{NN}} = 200$ GeV, Phys. Rev. Lett. **107**, 252301 (2011).

[10] C. Gale, S. Jeon, B. Schenke, P. Tribedy, and R. Venugopalan, Event-by-Event Anisotropic Flow in Heavy-Ion Collisions from Combined Tang-Mills and Viscous Fluid Dynamics, Phys. Rev. Lett. **110**, 012302 (2013).

[11] L. P. Csernai and D. Röhrich, Third flow component as QGP signal, Phys. Lett. B **458**, 454 (1999).

[12] J. Brachmann, S. Soff, A. Dumitru, H. Stöcker, J. A. Maruhn, W. Greiner, L. V. Bravina, and D. H. Rischke, Antiflow of nucleons at the softest point of the EoS, Phys. Rev. C **61**, 024909 (2000).

[13] L. Adamczyk *et al.* (STAR Collaboration), Beam-Energy Dependence of the Directed Flow of Protons, Antiprotons, and Pions in Au + Au Collisions, Phys. Rev. Lett. **112**, 162301 (2014).

[14] Y. Hirono, M. Hongo, and T. Hirano, Estimation of the electric conductivity of the quark gluon plasma via asymmetric heavy-ion collisions, Phys. Rev. C **90**, 021903 (2014).

[15] V. Voronyuk, V. D. Toneev, S. A. Voloshin, and W. Cassing, Charge-dependent directed flow in asymmetric nuclear collisions, Phys. Rev. C **90**, 064903 (2014).

[16] W. Deng and X. Huang, Electric fields and chiral magnetic effects in Cu + Au collisions, Phys. Lett. B **742**, 296 (2015).

[17] S. Pratt, Viewing the chemical volution of the quark-gluon plasma with charge balance functions, *Proceedings of 8th International Workshop on Critical Point and Onset of Deconfinement (CPOD 2013), in Napa, CA, USA*, 023.

[18] S. A. Bass, P. Danielewicz, and S. Pratt, Clocking Hadronization in Relativistic Heavy-Ion Collisions with Balance Functions, Phys. Rev. Lett. **85**, 2689 (2000).

[19] D. Kharzeev, R. D. Pisarski, and M. H. G. Tytgat, Possibility of Spontaneous Parity Violation in Hot QCD, Phys. Rev. Lett. **81**, 512 (1998).

[20] D. Kharzeev and R. D. Pisarski, Pionic measures of parity and *CP* violation in high-energy nuclear collisions, Phys. Rev. D **61**, 111901 (2000).

[21] D. E. Kharzeev and H. U. Yee, Chiral magnetic wave, Phys. Rev. D **83**, 085007 (2011).

[22] Y. Burnier, D. E. Kharzeev, J. Liao, and H. U. Yee, Chiral Magnetic Wave at Finite Baryon Density and the Electric Quadrupole Moment of Quark-Gluon Plasma in Heavy Ion Collisions, Phys. Rev. Lett. **107**, 052303 (2011).

[23] D. E. Kharzeev, J. Liao, S. A. Voloshin, and G. Wang, Chiral magnetic and vortical effects in high-energy nuclear collisions-A status report, Prog. Part. Nucl. Phys. **88**, 1 (2016).

[24] B. I. Abelev *et al.* (STAR Collaboration), Azimuthal Charged-Particle Correlations and Possible Local Strong Parity Violation, Phys. Rev. Lett. **103**, 251601 (2009).

[25] B. Abelev *et al.* (ALICE Collaboration), Charge Separation Relative to the Reaction Plane in Pb-Pb Collisions at $\sqrt{s_{NN}} = 2.76$ TeV, Phys. Rev. Lett. **110**, 012301 (2013).

[26] L. Adamczyk *et al.* (STAR Collaboration), Observation of Charge Asymmetry Dependence of Pion Elliptic Flow and the Possible Chiral Magnetic Wave in Heavy Ion Collisions, Phys. Rev. Lett. **114**, 252302 (2015).

[27] J. Adam *et al.* (ALICE Collaboration), Charge-dependent flow and the search for the chiral magnetic wave in Pb-Pb collisions at $\sqrt{s_{NN}} = 2.76$ TeV, Phys. Rev. C **93**, 044903 (2016).

[28] M. Anderson *et al.*, The Star time projection chamber: A unique tool for studying high multiplicity events at RHIC, Nucl. Instrum. Methods Phys. Res., Sect. A **499**, 659 (2003).

[29] W. J. Llope *et al.*, The STAR vertex position detector, Nucl. Instrum. Methods Phys. Res., Sect. A **759**, 23 (2014).

[30] M. L. Miller, K. Reygers, S. J. Sanders, and P. Steinberg, Glauber modeling in high-energy nuclear collisions, Annu. Rev. Nucl. Part. Sci. **57**, 205 (2007).

[31] L. Adamczyk *et al.* (STAR Collaboration), Inclusive charged hadron elliptic flow in Au + Au collisions at $\sqrt{s_{NN}} = 7.7$–39 GeV, Phys. Rev. C **86**, 054908 (2012).

[32] C. Adler, A. Denisov, E. Garcia, M. Murray, H. Strobele, and S. White, The RHIC zero degree calorimeters, Nucl. Instrum. Methods Phys. Res., Sect. A **461**, 337 (2001).

[33] J. Adams *et al.* (STAR Collaboration), Directed flow in Au + Au collisions at $\sqrt{s_{NN}} = 62.4$ GeV, Phys. Rev. C **73**, 034903 (2006).
[34] B. I. Abelev *et al.* (STAR Collaboration), System-Size Independence of Directed Flow Measured at the BNL Relativistic Heavy Ion Collider, Phys. Rev. Lett. **101**, 252301 (2008).
[35] S. A. Voloshin and T. Niida, Ultrarelativistic nuclear collisions: Direction of spectator flow Phys. Rev. C **94**, 021901 (R) (2016).
[36] A. M. Poskanzer and S. A. Voloshin, Methods for analyzing anisotropic flow in relativistic nuclear collisions, Phys. Rev. C **58**, 1671 (1998).
[37] D. Teaney and L. Yan, Triangularity and dipole asymmetry in relativistic heavy ion collisions, Phys. Rev. C **83**, 064904 (2011).
[38] M. Luzum and J. Y. Ollitrault, Directed Flow at Midrapidity in Heavy-Ion Collisions, Phys. Rev. Lett. **106**, 102301 (2011).
[39] B. Abelev *et al.* (ALICE Collaboration), Directed Flow of Charged Particles at Midrapidity Relative to the Spectator Plane in Pb + Pb Collisions at $\sqrt{s_{NN}} = 2.76$ TeV, Phys. Rev. Lett. **111**, 232302 (2013).
[40] C. A. Whitten (STAR Collaboration), The beam-beam counter: A local polarimeter at STAR, AIP Conf. Proc. **980**, 390 (2008).
[41] C. E. Allgower *et al.* (STAR Collaboration), The STAR endcap electromagnetic calorimeter, Nucl. Instrum. Methods Phys. Res., Sect. A **499**, 740 (2003).
[42] P. Bożek, Event-by-event viscous hydrodynamics for Cu-Au collisions at $\sqrt{s_{NN}} = 200$ GeV, Phys. Lett. B **717**, 287 (2012).
[43] U. W. Heinz and P. F. Kolb, Rapidity dependent momentum anisotropy at RHIC, J. Phys. G **30**, S1229 (2004).
[44] A. Adare *et al.* (PHENIX Collaboration), Measurements of directed, elliptic, and triangular flow in Cu + Au collisions at $\sqrt{s_{NN}} = 200$ GeV, Phys. Rev. C **94**, 054910 (2016).
[45] S. Gupta, The electrical conductivity and soft photon emissivity of the QCD plasma, Phys. Lett. B **597**, 57 (2004).
[46] G. Aarts, C. Allton, J. Foley, S. Hands, and S. Kim, Spectral Functions at Small Energies and the Electrical Conductivity in Hot Quenched Lattice QCD, Phys. Rev. Lett. **99**, 022002 (2007).
[47] P. Arnold, G. D. Moore, and L. G. Yaffe, Transport coefficients in high temperature gauge theories, 2. Beyond leading log, J. High Energy Phys. 05 (2003) 051.
[48] M. Greif, I. Bouras, C. Greiner, and Z. Xu, Electric conductivity of the quark-gluon plasma investigated using a perturbative QCD based parton cascade, Phys. Rev. D **90**, 094014 (2014).
[49] T. Steinert and W. Cassing, Electric and magnetic response of hot QCD matter, Phys. Rev. C **89**, 035203 (2014).
[50] L. McLerrana and V. Skokov, Comments about the electromagnetic field in heavy-ion collisions, Nucl. Phys. **A929**, 184 (2014).
[51] K. Tuchin, Time and space dependence of the electromagnetic field in relativistic heavy-ion collisions, Phys. Rev. C **88**, 024911 (2013).
[52] B. G. Zakharov, Electromagnetic response of quark-gluon plasma in heavy-ion collisions, Phys. Lett. B **737**, 262 (2014).
[53] HERAPDF1.5, https://www.desy.de/h1zeus/combined_results/herapdftable/.